frontiers in Mechanical Engineering

TYPE Original Research
PUBLISHED 03 June 2026
DOI 10.3389/fmech.2026.1783396

OPEN ACCESS

EDITED BY
Muhammad Umar Farooq,
University of Michigan, United States

REVIEWED BY
Mehdi Tlija,
King Saud University, Saudi Arabia
Chockalingam Palanisamy,
Multimedia University, Malaysia

*CORRESPONDENCE
Lu Che,
chelu9703@126.com

RECEIVED 08 January 2026
REVISED 11 May 2026
ACCEPTED 11 May 2026
PUBLISHED 03 June 2026

CITATION
Che L, Xu X, Mu W and Wang P (2026) Target product grabbing of factory robotic arm based on digital twin technology.
Front. Mech. Eng. 12:1783396.
doi: 10.3389/fmech.2026.1783396

Target product grabbing of factory robotic arm based on digital twin technology

Lu Che[1]*, Xin Xu[1], Weipeng Mu[1] and Peng Wang[2]

[1]College of Intelligent Manufacturing Engineering, Shanxi Institute of Science and Technology, Jincheng, China, [2]College of Automotive Engineering, Jilin University, Changchun, China

Introduction: As smart manufacturing upgrades to flexibility and precision, factory robotic arm target grabbing is the core link of material transfer in the production line, and its performance directly determines production efficiency and product quality. However, the current factory robotic arms have insufficient gripping accuracy for target products and have weak anti-interference capabilities. Therefore, the study proposes a factory robotic arm target product grabbing model based on digital twin technology, aiming to break through the accuracy and anti-interference bottlenecks through virtual and real collaborative optimization.
Methods: The research first builds a cross-platform communication mechanism between the robot operating system and Unity3D, and encapsulates the underlying protocol through rosSocket middleware. Secondly, a high-fidelity digital twin is built through SolidWorks modeling, 3DMax rendering and Unity3D assembly. The three-dimensional bounding box projection collision detection algorithm is combined to improve planning efficiency. Finally, the Rapidly-exploring Random Tree-Connect algorithm and tool center point calibration technology are integrated to build a composite grabbing model.
Results: Experimental results showed that the average coordinate deviation of the center point of the proposed model tool was 2.34 mm. The capture success rate in normal scenarios was 90%, and the success rate in complex scenarios was 80%, which was 10% and 20% higher than that of mainstream deep reinforcement learning methods. The grabbing efficiency was 19.1% higher than that of the point cloud segmentation method, and the energy consumption and fixture wear rate were 25% and 47% lower than those of the traditional method.
Discussion: This model achieves collaborative improvements in accuracy, efficiency, and economy through virtual and real collaborative optimization.

KEYWORDS
digital twin technology, industry, robotic arm, RRT-connect, Unity3D

1 Introduction

Under the strategic guidance of the "14th Five-Year Plan" for Intelligent Manufacturing Development, the manufacturing industry is accelerating its transformation to digitalization, networking, and intelligence, with the flexible upgrade of factory automation production lines becoming a core breakthrough direction (Gao and Lu, 2024; Peng et al., 2024). As the core execution unit of the production line in material transfer, assembly and testing, the robotic arm's accuracy and efficiency in grabbing target products directly determines the production rhythm, product qualification rate and operating costs, which is one of the key indicators to measure the intelligent manufacturing (Touhid et al., 2023; Tsakoumis et al., 2025). Especially in precision operation scenarios such as electronic manufacturing and automobile parts assembly, the requirements for robotic arm grabbing accuracy have increased to within ±3 mm. Meanwhile, they need to adapt to complex working conditions such as switching between multiple types of workpieces and random stacking. Traditional grabbing technology has gradually exposed insurmountable bottlenecks (Chen et al., 2025; Liao and Cai, 2024). According to the ISO 23247 "Digital Twin Framework for Manufacturing Systems" standard, digital twin systems need to achieve precise mapping, real-time interaction, and collaborative optimization between physical entities and virtual models, providing standardized architecture support for flexible production in the manufacturing industry. As the core execution link of intelligent manufacturing, the technological upgrade of the robotic arm grasping system needs to strictly comply with the core requirements of this standard framework.

As the core technology to realize real-time mapping and collaborative optimization of the physical world and the virtual world, digital twin technology provides a new technical path to solve robotic arm grabbing (Yang et al., 2024). The academic community has conducted extensive targeted research on the application of this technology in the field of robotic arm grabbing, and has achieved a series of breakthrough results. In response to problems such as trajectory conflicts and coordination imbalances that are prone to occur in multi-robot collaborative grabbing scenarios, Duan et al. built a digital twin monitoring framework for dual-robot collaborative operations. The results showed that this framework could effectively avoid physical collisions and greatly improve the stability of dual robotic arms in collaborative operations such as assembly and transportation (Duan et al., 2023). To optimize the positioning accuracy of the robotic arm, Wu et al. proposed a digital twin-driven three-dimensional position information interaction and positioning error compensation method. This method built a three-dimensional position information interaction mechanism that combined virtual and real conditions to provide real-time feedback on the relative pose data of the robotic arm end effector and the target workpiece (Wu et al., 2023). Faced with the poor adaptability of robotic arms in grabbing under multiple varieties and changing working conditions, Ren et al. proposed a robot system that integrated continuous learning mechanisms and digital twins. The experiments proved that this system could effectively improve the target recognition and capture success rate of robotic arms under complex working conditions such as random stacking and partial occlusion. It solved re-adjusting parameters and long adaptation cycles when switching scenarios in traditional grabbing systems (Ren et al., 2023). The style planner has become the mainstream technology for path planning of digital twin driven robotic arms due to its good real-time performance and adaptability to complex constraints. The Rapidly-exploring Random Tree (RRT) algorithm and its improved algorithms are widely used. In existing research, scholars have optimized RRT algorithm, such as improving the sampling strategy to enhance search efficiency and using curve fitting to optimize path smoothness, but there are generally core bottlenecks. The paths generated by traditional RRT algorithms are tortuous and have poor smoothness, and in digital twin virtual real collaborative scenarios, the synergy between path planning and virtual real data interaction is insufficient, making it difficult to balance capture efficiency and trajectory smoothness. Although the RRT-Connect algorithm improves path search efficiency through bidirectional extension, there are still path redundancy and poor connection with end precision calibration in complex working conditions.

Overall, although existing research has achieved technological breakthroughs in specific scenarios, there are still clear technical bottlenecks. Firstly, the real-time performance of cross platform virtual and real data interaction is insufficient, and the current mainstream cross platform communication methods have obvious performance shortcomings. The throughput of WebSocket protocol is limited, and the end-to-end delay of ROS Tool Center Point (TCP) connector in precision grasping scenarios is difficult to control within 100 ms, which cannot meet the real-time requirements of ± 3 mm precision grasping of robotic arms. Although MQTT protocol has low latency, it is prone to packet loss problems in concurrent transmission of multiple data, resulting in asynchronous virtual and real motion states. Secondly, the high fidelity of twin body modeling is insufficient, and existing modeling methods often use a single toolchain, which makes it difficult to accurately map the kinematic and dynamic characteristics of the robotic arm, resulting in deviations between virtual simulation and physical reality, and unable to effectively support offline path planning and error calibration. Thirdly, there is insufficient composite optimization of grasping strategies under complex working conditions. Existing research has failed to integrate sampling style path planning with end precision calibration depth, and has not solved the problem of poor smoothness of RRT algorithm paths, making it difficult to adapt to complex grasping conditions such as multiple varieties and random stacking.

Therefore, a factory robotic arm target product grasping model based on digital twin technology is proposed, strictly following the ISO 23247 digital twin framework requirements, aiming to provide technical support for the precision and efficiency of robotic arm grasping in flexible production lines. The innovation of the research lies in constructing a cross-platform optimized communication mechanism between Robot Operating System (ROS) and Unity3D, optimizing the communication protocol to reduce end-to-end latency to within 80 ms, and solving the insufficient real-time performance of existing communication methods. A digital mapping method for SolidWorks, 3DMax, and Unity3D multi-toolchain collaboration is designed, accurately replicating the kinematic and dynamic characteristics of the robotic arm, and constructing high fidelity robotic arm twins. The RRT-Connect path planning algorithm is combined with TCP calibration technology to optimize path smoothing strategy, forming a composite grasping strategy of perception, planning, calibration, and execution, and solving the uneven path and insufficient grasping accuracy in traditional RRT algorithm.

2 Methods

2.1 Visual communication mechanism between Unity3D virtual scene and ROS

To achieve precise collaboration between virtual scenarios and physical hardware, the research uses ROS as a heterogeneous component collaboration framework to build an information

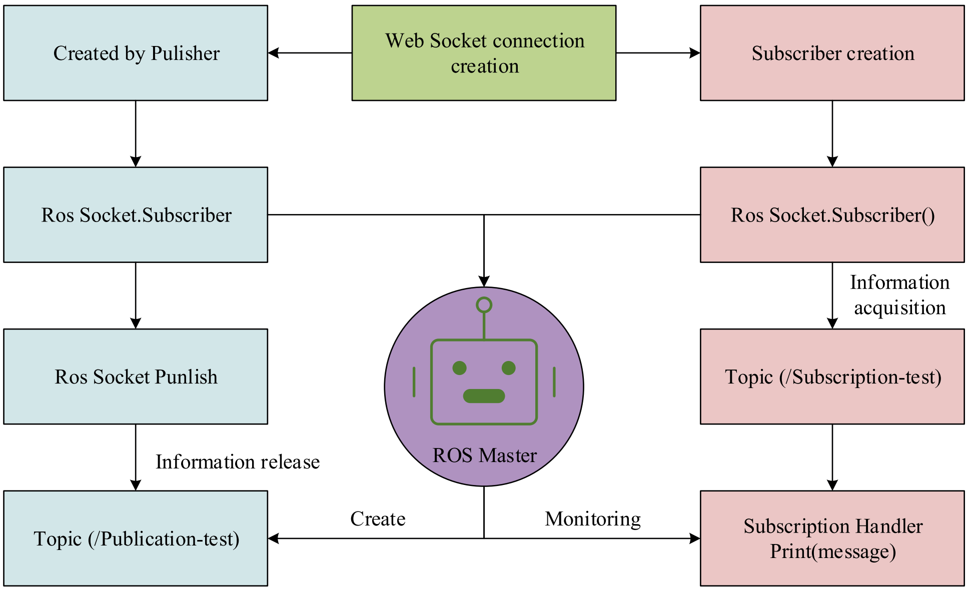

FIGURE 1
Unity3D communication node creation process.

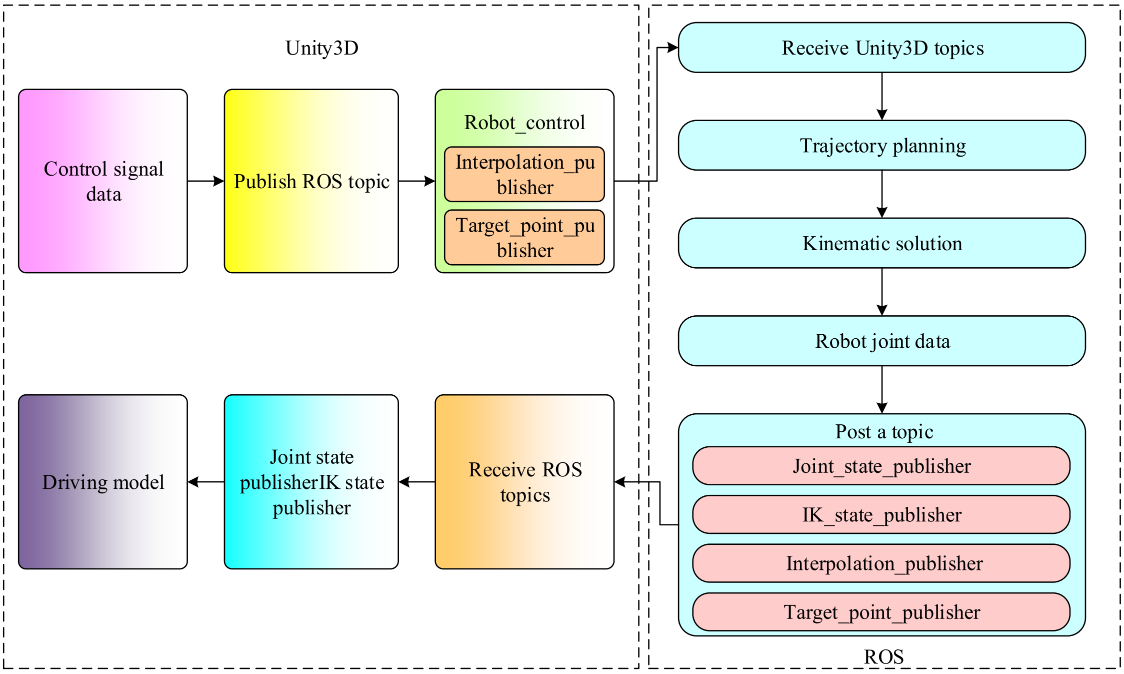

FIGURE 2
Flowchart of Unity3D and ROS integration model.

interaction channel between Unity3D and robot hardware systems (Wang et al., 2023). The construction of Unity3D communication nodes is the core technical support, and its specific process is shown in Figure 1.

From Figure 1, the core logic of the cross-platform message interaction between the Unity3D environment and the ROS revolves around the distributed communication mechanism of ROS. The asynchronous transmission of data is completed through the publish and subscribe modes. In the process, ROS Master, as the core coordination component, is responsible for the registration and node matching functions of Topic resources. When the Publisher node calls the Advertise method through rosSocket, the ROS Master will create the publication test Topic and register the publisher information. After the Subscriber node initiates a subscription

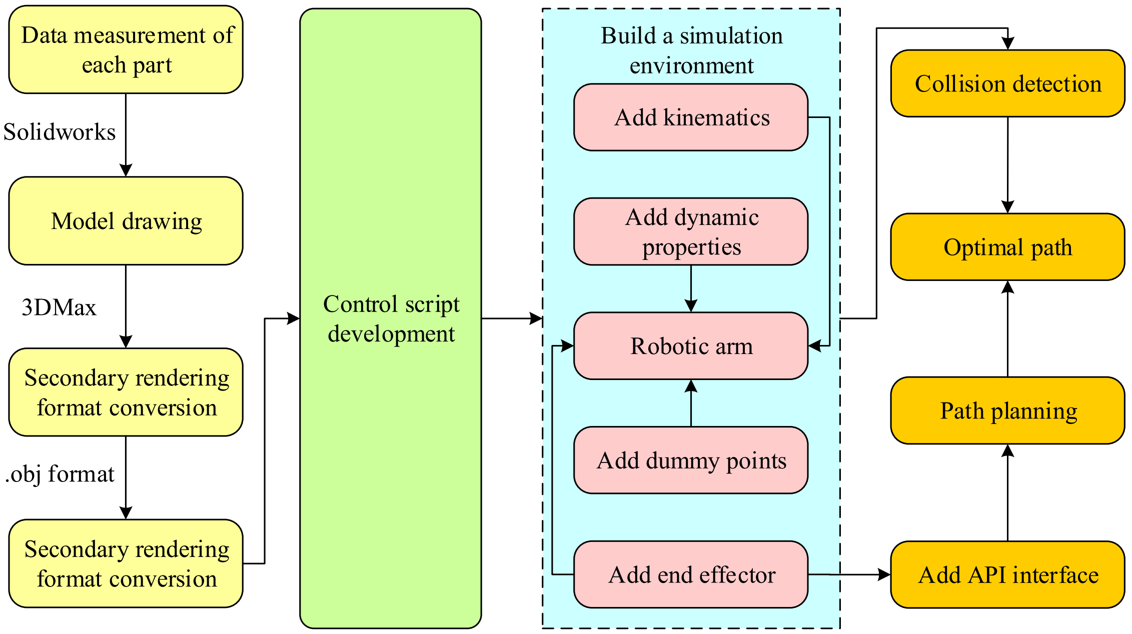

FIGURE 3
Digital twin motion planning framework.

request through the Subscribe method, the ROS Master will associate it with the corresponding Topic to achieve decoupled communication between the publisher and the subscriber (Rivera-Pinto et al., 2024). As the communication middleware between Unity and ROS, rosSocket encapsulates the details of network communication, so that Unity does not need to directly process the underlying protocol of ROS, and can send and receive messages through simple interface calls. For the subscriber process, the IP and port configuration connected by WebSocket are the prerequisite for cross-process communication, and the callback mechanism of Subscription Handler ensures real-time processing after message reception, which conforms to the characteristics of ROS asynchronous communication and adapts to Unity's component development logic. To coordinate virtual and real motion states of the robotic arm, the research integrates Unity3D and ROS. The integrated model process is shown in Figure 2.

From Figure 2, at the data flow level, Unity3D is the visual carrier of the virtual model, which first generates control signal data, and completes the instruction issuance through topics such as robot_control, Interpolation_publisher, and Target_point_publisher. The ROS serves as the decision-making layer of motion control. After receiving the above topic data, it sequentially executes trajectory planning and kinematics solving, converting abstract control instructions into specific motion parameters in the robot joint space (Jiao et al., 2025). The ROS transmits the solved robot joint data and inverse kinematics state back to Unity3D through the Joint_state_publisher and IK_state_publisher topics. After Unity3D subscribes to this type of topic, it calls the driving logic corresponding to Joint_state_publisher and IK_state_publisher to complete the motion state synchronization of the virtual model. Topic-based decoupled communication not only retains the algorithmic advantages of ROS in the field of robot motion planning, but also takes advantage of the characteristics of Unity3D in virtual model visualization and interactive development, realizing virtual and real linkage in which virtual instructions drive actual movement and actual status feedback virtual performance.

2.2 Digital twin-driven robotic arm grabbing motion planning framework

To achieve precise planning and risk control for factory robotic arm target grabbing, the study builds a digital twin motion planning framework through three links: digital mapping, virtual function empowerment and motion planning verification to achieve offline optimization and online monitoring of the grabbing process. The digital twin motion planning framework is shown in Figure 3.

From Figure 3, the framework first completes the digital mapping of the robotic arm through a multi-tool chain. SolidWorks is used to achieve precise modeling of physical parts, which is converted into Unity3D-compatible. Obj format after 3DMax rendering optimization. Finally, Unity3D is used to complete virtual scene construction, script development and virtual assembly of the robotic arm, transforming the physical robotic arm into a digital twin. At the virtual model functional layer, by adding kinematic characteristics, dynamic characteristics, dummy positioning points, end effectors and API interfaces, the digital twin and the physical robotic arm are given consistent motion constraints and execution capabilities, providing a high-fidelity virtual carrier for subsequent grabbing motion planning (Dawn et al., 2024). Collision detection avoids the interference between the robotic arm, the workpiece, and the environment. Path planning initially generates the grabbing trajectory. Optimal path solution further improves the efficiency and stability of the grabbing action.

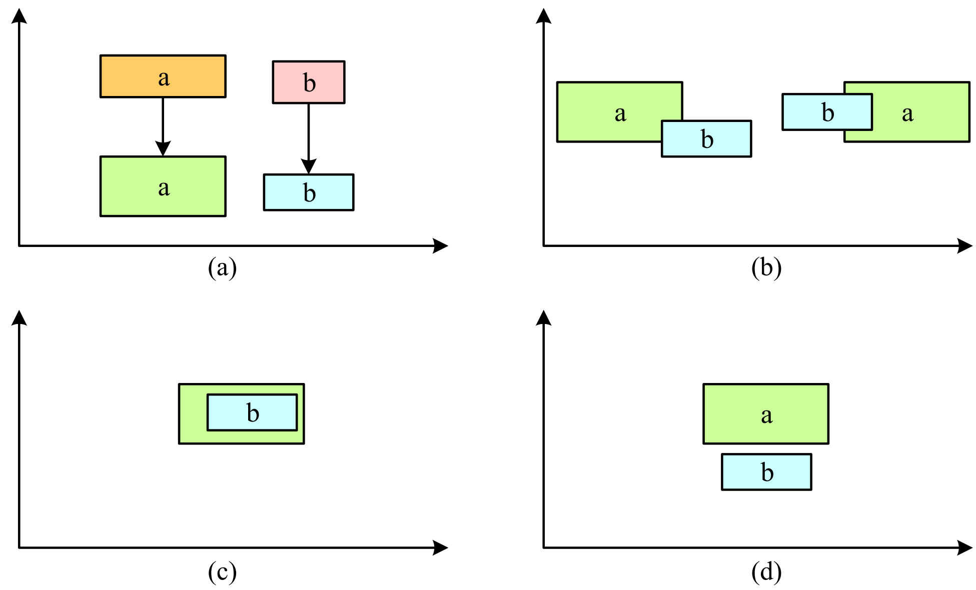

FIGURE 4
Typical status of bounding box collision. **(a)** Bounding box projection. **(b)** Intersect. **(c)** Embed. **(d)** No collision.

Collision detection uses a three-dimensional bounding box projection algorithm to convert complex three-dimensional space collision judgment into two-dimensional plane feature verification to improve computing efficiency (Singh and Ray, 2024). The coordinate expressions of components A and B in the three-dimensional coordinate system are shown in Equation 1.

$$\begin{aligned} A &= \{x_a, y_a, z_a\} \\ B &= \{x_b, y_b, z_b\} \end{aligned} \tag{1}$$

In Equation 1, $\begin{aligned} A &= \{x_a, y_a, z_a\} \\ B &= \{x_b, y_b, z_b\} \end{aligned}$ represents the coordinate value of component A in the x-axis, y-axis, and z-axis directions. $\{x_b, y_b, z_b\}$ represents the coordinate value of component B in the x-axis, y-axis, and z-axis directions. To define the space occupation range of components, a bounding box parameter model is constructed, as shown in Equation 2.

$$\begin{cases} x_{a-MIN} \le x_b \le x_{a-MAX} \\ y_{a-MIN} \le y_b \le y_{a-MAX} \\ z_{a-MIN} \le z_b \le z_{a-MAX} \end{cases} \tag{2}$$

In Equation 2, x_{a-MIN} and x_{a-MAX} represent the minimum and maximum coordinates of component A in the x-axis. y_{a-MIN} and y_{a-MAX} represent the minimum and maximum coordinates of component A in the y-axis. z_{a-MIN} and z_{a-MAX} represent the minimum and maximum coordinates of component A in the z-axis (Wang et al., 2025). The typical state of bounding box collision is shown in Figure 4.

Figure 4a is a schematic diagram of the bounding box projection. From Figure 4a, the projection range of the bounding boxes of components a and b on the two-dimensional plane is the geometric basis for collision determination. Figure 4b is a schematic diagram of intersection. From Figure 4b, the projections of the bounding boxes of the two objects have overlapping areas, and this overlap meets the conditions for the intersection of at least two plane projections, corresponding to the collision state in the actual scene. Figure 4c is a schematic diagram of embedding. From Figure 4c, the bounding box of one object is completely contained within the projection of the bounding box of another object, which is a special form of collision state. Figure 4d is a collision-free schematic diagram. From Figure 4d, the projections of the bounding boxes of the two objects have no overlapping areas, which is consistent with the collision-free spatial position relationship. Although the 3D bounding box projection algorithm can improve computational efficiency, due to its simple geometric approximation structure, it is prone to collision false alarms caused by overlapping bounding box angles, which can interfere with the continuity of the grasping process. In response to this, a layered collision detection optimization strategy is proposed, which improves detection accuracy while retaining efficiency advantages through two-stage verification of coarse and fine screening. In the coarse screening stage, the original 3D bounding box projection algorithm is used to quickly screen the robotic arm, workpiece, and static obstacles, eliminate collision free objects to reduce computational complexity, and ensure real-time performance. In the fine screening stage, for suspected collision pairs with overlapping bounding boxes, a grid grid collision detection algorithm is introduced for secondary verification, and false alarms are eliminated by comparing the actual grid spatial coordinates of the components. To balance accuracy and efficiency, the mesh model is lightweight processed, simplifying the number of faces while retaining core features, ensuring that the end-to-end delay of fine screening is ≤50 ms and does not affect the real-time response of grasping. This hierarchical logic is embedded in the Unity3D virtual scene script, which is linked to the kinematic and dynamic characteristics of the robotic arm twin. When there is a false alarm, the original trajectory is maintained. When there is a real collision, path re-planning is triggered.

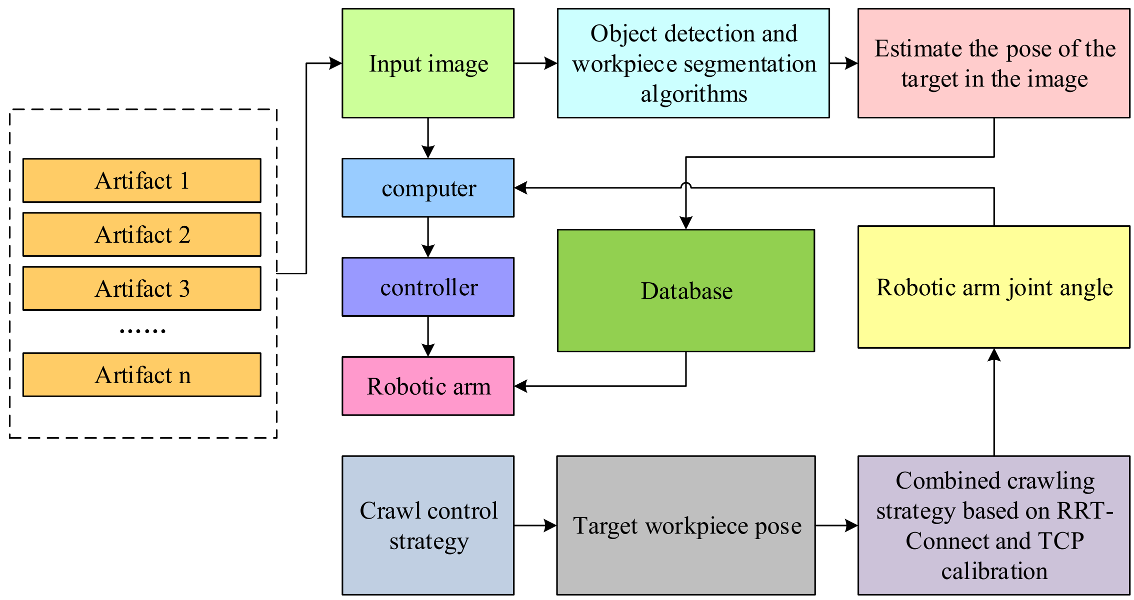

FIGURE 5
Flowchart of factory robotic arm target product grabbing model based on digital twin technology.

2.3 Factory robotic arm target product grabbing model based on digital twin technology

To accurately and efficiently grasp target products by robotic arms in factory scenarios, a grabbing model based on digital twin technology is constructed. This model integrates the three-level architecture of perception, decision-making, and execution to form a closed-loop control system. Its flow chart is shown in Figure 5.

From Figure 5, the model completes the pose estimation of the target in the image by combining the input image with target detection and workpiece segmentation algorithms. At the decision-making and planning level, the process integrates the RRT and the combined grabbing strategy calibrated by TCP. The execution control layer issues the planned joint angle instructions to the robotic arm through the collaboration of the computer and the controller, and combines the grabbing control strategy to complete automated grabbing operations for multiple types of workpieces (Stan et al., 2023). The coordinate transformation of the end of the robotic arm relative to the base coordinate is essentially a series transformation process of the multi-joint coordinate system. The robotic arm contains n rotating joints. The homogeneous transformation matrix of the local coordinate system of the i-th joint relative to the coordinate system of the $i-1$-th joint is $T_{i(i-1)}$. The homogeneous transformation matrix T_{0n} of the end effector relative to the base coordinate system is the product of the transformation matrices of each joint. Its general form is shown in Equation 3.

$$T_{i(i-1)} = \begin{bmatrix} R_i & t_i \\ 0 & 1 \end{bmatrix} \tag{3}$$

In Equation 3, R_i is the rotation matrix of the i-th joint. R_i is the translation vector of the i-th joint, 0 is the zero vector of 3×1, and 1 is the normalization coefficient of the homogeneous coordinates. During the operation of the robotic arm, key sensor data such as torque, actual position, and speed are collected in real time and fed back to the digital twin virtual model through a high-frequency data transmission link (transmission frequency ≥100 Hz). The physics based simulation parameters are dynamically updated to achieve high-frequency bidirectional synchronization between the virtual twin and the physical robotic arm, ensuring high consistency between virtual simulation and physical reality. Based on the updated virtual model, real-time simulation and fault prediction of the grasping process are carried out to accurately identify potential joint jamming, torque overload, positioning deviation and other fault risks. Before the fault occurs in the physical world, automatic feedback adjustment signals are sent to the decision-making planning layer to correct joint motion parameters and grasping strategies, achieving early prevention and control of faults and significantly improving the stability and reliability of the grasping process. During the actual calibration process, the known pose data of the end effector in the base coordinate system is collected through three-point/four-point calibration methods, and then substituted into the above transformation model to back-solve the actual geometric parameters of each joint, thereby correcting the error between the theoretical model and the physical robotic arm, and improving the positioning accuracy of the end effector (Inamura, 2023).

To clearly explain the calibration principle, the study uses the two-point calibration method as an example to conduct mathematical derivation. The robotic arm is controlled to make the end calibration pin contact the same fixed calibration point Q_T in two different postures. The pose constraint equation is shown in Equation 4.

$$\begin{cases} R_1 P_E + Q_1 = Q_T \\ R_2 P_E + Q_2 = Q_T \end{cases} \tag{4}$$

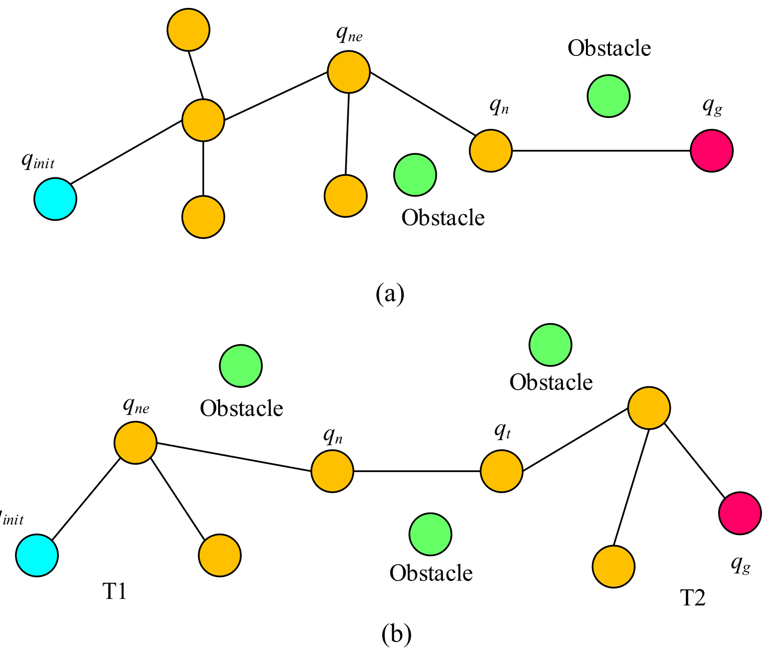

FIGURE 6
RRT and RRT-Connect path planning diagram. **(a)** Schematic diagram of RRT path planning. **(b)** RRT Connect path planning diagram.

In Equation 4, R_1 and Q_1 represent the rotation matrix and position at the end in posture 1. R_2 and Q_2 represent the rotation matrix and position at the end in posture 2. P_E represents the position of the TCP to be found in the terminal coordinate system. Q_T represents the position of the fixed calibration point in the base coordinate system. After eliminating the known quantity Q_T, the position solution equation is obtained, as shown in Equation 5.

$$R_1 P_E - R_2 P_E = Q_2 - Q_1 \tag{5}$$

For scenarios requiring higher accuracy, n-order calibration is used to construct an overdetermined system of equations, and redundant constraints are used to improve the solution accuracy. Its general form is shown in Equation 6.

$$\begin{cases} R_1 P_{TCP} + E_1 = Q_T \\ R_2 P_{TCP} + E_2 = Q_T \\ R_3 P_{TCP} + E_3 = Q_T \\ \vdots \\ R_n P_{TCP} + E_n = Q_T \end{cases} \tag{6}$$

In Equation 6, E_i is the position of the origin of the end coordinate system in the base coordinate system during the i-th measurement. P_{TCP} indicates the position of the TCP to be found in the terminal coordinate system. To further improve the overall motion accuracy of the robotic arm and achieve precise calibration of internal geometric parameters of each joint, external laser tracking technology is introduced to capture real-time spatial position and attitude data of the end effector of the robotic arm. During the calibration process, the laser tracker target is fixed to the end of the robotic arm, and the robotic arm is controlled to complete multi-pose and multi-position movements according to a preset trajectory, synchronously collecting joint angle data and actual end pose data. By combining the Denavit Hartenberg parameter model, the collected measured data is compared with theoretical simulation data to construct joint geometry error constraint equations, and the core geometric parameter deviations such as length and offset of each joint are inversely solved. By iteratively optimizing algorithms to correct parameter errors and updating the joint parameters of the digital twin virtual model, high-precision matching between the virtual model and the physical robotic arm can be achieved, significantly reducing the impact of joint geometry errors on end effector positioning accuracy and meeting the precision requirements of precision grasping scenarios in factories. The RRT algorithm is the core technology for path planning in complex environments. It achieves collision-free path search through random sampling and tree expansion. The RRT-Connect algorithm further improves efficiency through bidirectional expansion. The schematic diagram of RRT and RRT-Connect path planning is shown in Figure 6.

Figure 6a is a schematic diagram of RRT path planning. From Figure 6a, with the initial configuration q_{init} and the target configuration q_g as endpoints, configuration points are generated through random sampling. The node q_{ne} closest to q_{rand} is searched in the grown tree T, and a new node q_n is generated with a fixed step size along the q_{ne} to q_{rand} direction. If there is no collision on the path from q_{ne} to q_n, q_n is added to tree T. The above process is repeated until the tree extends to q_g. The expression of the node q_{ne} closest to q_{rand} in the tree is shown in Equation 7.

$$q_{ne} = \arg \min_{q \in T} - \text{Distance}(q, q_{rand}) \tag{7}$$

The distance function $\text{Distance}(q_a, q_b)$ between two points q_a and q_b is shown in Equation 8.

$$\text{Distance}(q_a, q_b) = \|q_a - q_b\| = \sqrt{\sum_{i=1}^{n} (q_a^i - q_b^i)^2} \tag{8}$$

In Equation 8, q_a^i and q_b^i represent the i-th component of the configuration vectors q_a and q_b. The new node q_n obtained by extending one step from q_{ne} to q_{rand} is shown in Equation 9.

$$q_n = q_{ne} + \delta \frac{q_{rand} - q_{ne}}{\|q_{rand} - q_{ne}\|} \tag{9}$$

In Equation 9, δ represents the step size. Figure 6b is a schematic diagram of RRT-Connect path planning. From Figure 6b, the RRT-Connect algorithm adopts a two-way expansion strategy and simultaneously grows two trees T1 and T2 from the initial configuration point q_{init} and the target configuration point q_g, and attempts to connect the two trees during each expansion. When a new node of a tree falls within the re-connection radius r of another tree, the expression of nearby node search is shown in Equation 10.

$$q_{ne} = \{q \in T \mid \text{Distance}(q, q_n) \le r\} \tag{10}$$

After connection, the path is optimized through the optimal parent node selection strategy to improve path smoothness and execution efficiency. The expression of selecting the optimal parent node candidate $q_{\min}$ is shown in Equation 11.

$$q_{\min} = \arg\min_{q \in q_{ne}} [\text{Cos}\,t(q) + \text{Distance}(q, q_n)] \tag{11}$$

In Equation 11, $\text{Cos}\,t(q)$ represents the cumulative path cost from the starting point q_{init} to the node q.

3 Results and analysis

3.1 Performance test of factory robotic arm target product grabbing model based on digital twin technology

To verify the motion performance advantages of the proposed digital twin grasping model and clarify the impact of path constraints on performance, the RRT algorithm was selected as the comparison benchmark. The core parameters of the RRT and RRT-Connect algorithms are set uniformly, the fixed expansion step is planned to be 15 mm, and the RRT-Connect bidirectional tree re-connection radius threshold is set to 25 mm. The experimental configuration is as follows. The hardware of the robotic arm adopts the Oudeji JL8-600 6-degree-of-freedom serial industrial robotic arm, with a rated load of 1 kg, a repeatability accuracy of ±0.05 mm, and a maximum joint movement speed of 4,000 mm/s (joint 1–2) and 800 mm/s (joint 3), suitable for factory light load grasping scenarios. The rotation angle of each joint is dynamically set based on the target workpiece position, with a range of-180° to 180°. Define the complexity of obstacle environments, simulate actual light load grasping scenarios in factories, set up three types of static obstacles (with sizes of 100 mm × 80 mm × 50 mm, 80 mm × 60 mm × 40 mm, 60 mm × 50 mm × 30 mm), randomly distributed in the motion space of the robotic arm, with obstacle spacing ≥150 mm, and simulate interference factors such as material racks and auxiliary fixtures in the factory production line. The test equipment is based on "Robot Integrated Joint Performance and Test Methods" (GB/T 43200-2023), equipped with a rotational speed sensor with an accuracy of ±0.1%, an angle sensor with an accuracy of ±2arcsec, and a data acquisition system with a sampling frequency of 1 kHz. The temperature of the experimental environment is 15–35 °C, and the relative humidity is 25%–75%. The function of the j4 and j5 joints is the attitude orientation and fine-tuning of the end effector. They are mainly responsible for adjusting the end grasping angle to adapt to the attitude of the workpiece. Their motion range and angular velocity are much smaller than those of the j1-j3 and j joints. In the light load grasping scenario, the j4 and j5 joints always maintain small and smooth movements without obvious fluctuations and impacts. The impact on the stability of the overall motion is negligible, so the analysis will not be carried out. The joint angular velocity measurement results are shown in Figure 7.

Figure 7a shows the RRT joint angular velocity measurement results. From Figure 7a, during the 0–15 s test period, the angular velocity of the j1 changed with time without fluctuations. The angular velocity of the j2, j3, and j6 fluctuated violently with time, and the high-frequency jitter was significant, with an amplitude range of 0–60°/s. Figure 7b shows the joint angular velocity measurement results of the proposed model. From Figure 7b, the angular velocity curve of the j1 remained stable over time. Compared with the RRT joint angular velocity measurement, the smoothness of the j2 and j3 was significantly improved, and the amplitude narrowed to 0–15°/s. The proposed model achieves rapid convergence through the pre-planning and trajectory smoothing constraints, and effectively suppresses speed mutations. The joint angular acceleration measurement results are shown in Figure 8.

Figure 8a shows the RRT joint angular acceleration measurement results. From Figure 8a, in addition to the j1, the angular acceleration curves of the j2, j3, and j6 fluctuated extremely violently with time. The amplitude of the joint angular acceleration ranged from −500° to 500°/s². Multiple pulse oscillations occur, reflecting the strong impact characteristics of joint motion. Long-term operation can easily aggravate the wear of the robotic arm joints. Figure 8b shows the joint angular acceleration measurement results of the proposed model. From Figure 8b, the amplitude of the angular acceleration of the j1, j2, j3, and j6 has greatly reduced over time, converging to the −300–300°/s², and the oscillation frequency and amplitude have significantly reduced. This is due to the collision detection and trajectory optimization completed in advance by the digital twin model in the virtual environment, which reduces the dynamic impact of the physical robotic arm. The measurement results of joint angular rotation speed are shown in Figure 9.

Figure 9a shows the measurement results of the RRT joint rotation speed. From Figure 9a, the rotation speed of the four joints j1, j2, j3, and j6 fluctuated greatly with time, ranging from −10° to 10°/s. The high-frequency oscillation was frequent, and the speed changes between joints were not synchronized, and the movement coordination was poor, which could easily lead to positioning errors of the end effector. Figure 9b shows the joint rotation speed measurement results of the research model. From Figure 9b, the rotation speed of the j1 changed smoothly with time. The fluctuation range of the rotation speed of the j1, j2, j3, and j6 was greatly narrowed and remains at −7~6°/s. It was stable in the later

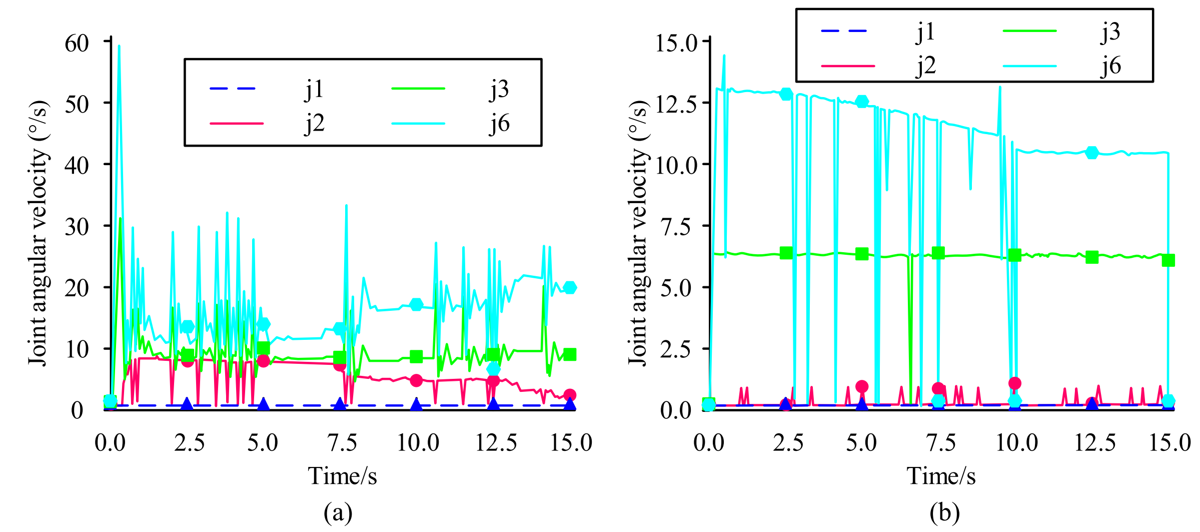

FIGURE 7
Joint angular velocity measurement results. **(a)** RRT joint angular velocity measurement. **(b)** Joint angular velocity measurement of the proposed mod.

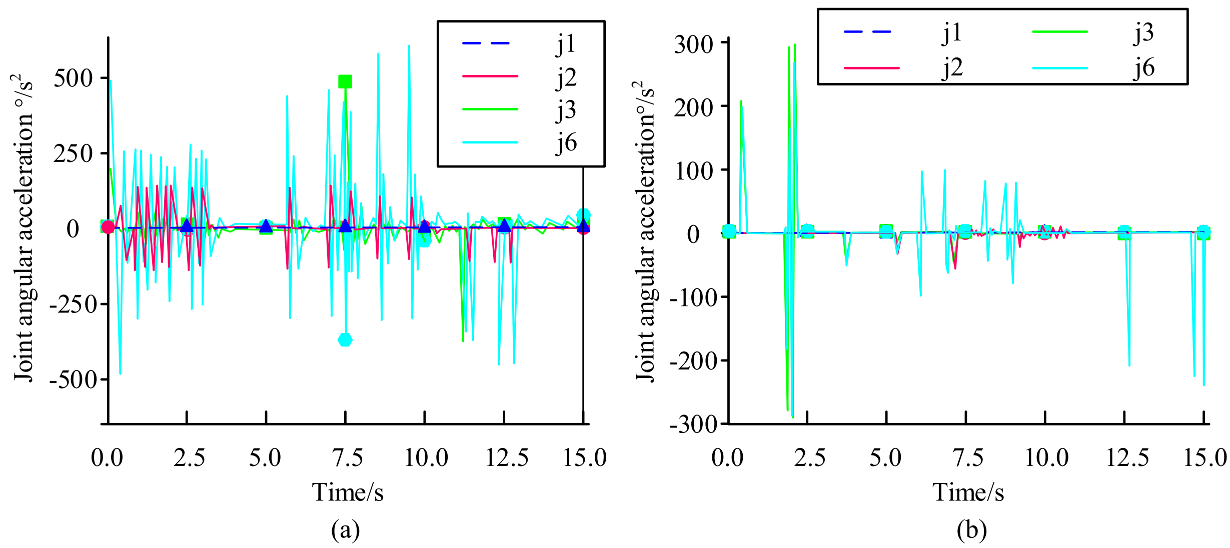

FIGURE 8
Joint angular acceleration measurement results. **(a)** RRT joint angular acceleration measurement. **(b)** Joint angular acceleration measurement of the proposed model.

period. The consistency and smoothness of the joint motion are significantly improved, adapting to the high-precision grabbing requirements of various types of workpieces in the factory. In order to clarify the source of the performance improvement of the proposed model and clarify whether the improvement effect comes from the RRT-Connect algorithm itself and the DT bidirectional synchronization mechanism, a control variable ablation experiment was designed. The joint angular velocity fluctuation amplitude, joint angular acceleration peak value, and joint rotation speed standard deviation were used as core evaluation indicators to compare with the baseline RRT algorithm. All improvement modules are explicitly defined, and there are no undisclosed hidden trajectory smoothing strategies. Each group of ablation experiments was run repeatedly 30 times, and the data were the mean ± standard deviation of 30 experiments. An independent sample t-test was used for statistical significance analysis, and the significance level $\alpha = 0.05$ was set to verify the statistical significance of the performance differences between each group. The experimental results are shown in Table 1.

From Table 1, compared with the baseline RRT algorithm, all indicators of the RRT-Connect group were significantly optimized, $p = 0.032 < 0.05$, and the difference was statistically significant,

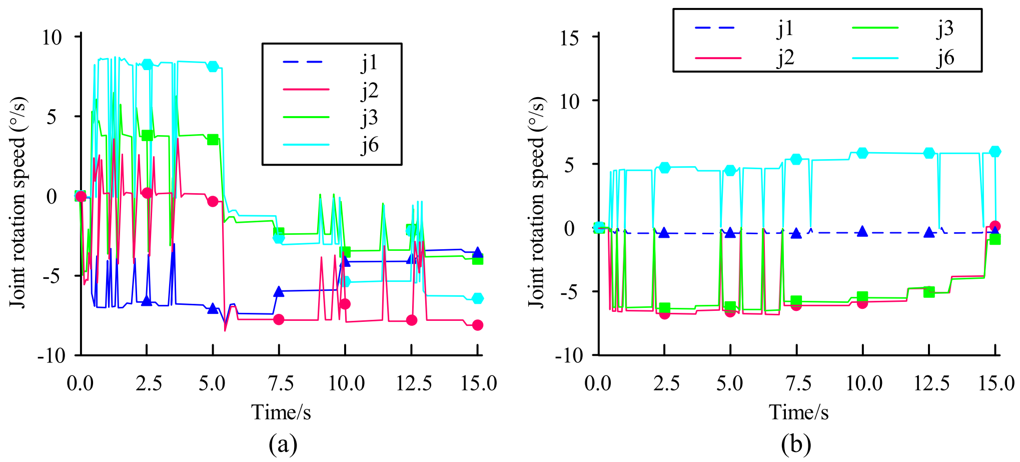

FIGURE 9
Measurement results of joint angular rotation speed. **(a)** RRT joint rotation speed measurement. **(b)** Joint rotation speed measurement of the proposed model.

TABLE 1 **Ablation experiment.**

Experimental group	Joint angular velocity fluctuation amplitude (°/s)	Peak joint angular acceleration (°/s2)	Standard deviation of joint rotation speed (°/s)	Statistical significance (*p*-value) with RRT algorithm
RRT algorithm	58.6 ± 3.2	±492.5 ± 18.7	1.85 ± 0.21	—
RRT-connect	41.8 ± 2.7	±408.3 ± 15.2	1.33 ± 0.17	0.032*
RRT-connect + DT synchronization	25.7 ± 2.1	±357.6 ± 12.9	0.96 ± 0.13	0.008**

* indicates p < 0.05; ** indicates p < 0.01.

indicating that its two-way expansion strategy can effectively improve motion stability. The optimization effect of the RRT-Connect + DT synchronization group was more significant, p = 0.008 < 0.01, and the difference was extremely significant. The angular velocity fluctuation and angular acceleration peak value decreased by 56.1% and 27.4%, respectively, and the standard deviation of the rotation speed decreased by 48.1%. The experimental results clearly verify that the model performance improvement is due to the synergy between the RRT-Connect algorithm and the DT two-way synchronization mechanism. The reliability of the statistical data of 30 repeated tests was in line with the advanced robot path planning experimental specifications.

3.2 Practical application of factory robotic arm target product grabbing model based on digital twin technology

To verify the accuracy and stability of the TCP calibration technology in the digital twin model, multiple sets of repeated calibration experiments were designed, and the four-point calibration method was used to collect calibration point data. In the experiment, the KEYENCE 3D laser tracker VL-800 series was used to collect the coordinates of calibration points, and each group of tests independently adjusted the robotic arm attitude and data recording. The VL-800 series has a measurement speed of 8 s per scan, a scanning accuracy of 2 microns, a resolution of 9 million points, a maximum scanning range of W580 × D300 × H200 mm, a single scan speed of 8 s per scan, a single scan accuracy of 2 microns, an operating system of Windows 10 Professional/Enterprise * 1 Windows 11 Professional/Enterprise * 1, and a host weight of 51.1 kg. The experimental results are shown in Table 2.

According to Table 1, the two test deviations of four calibration points and TCP were calculated using the two norm method. The deviations of calibration points 1-4 were approximately 2.48 mm, 1.03 mm, 1.85 mm, and 1.09 mm, respectively, all at a relatively low level. The TCP deviation was about 4.88 mm, which exceeded the accuracy requirement of ± 3 mm for industrial grasping positioning. To further verify the applicability in actual production scenarios, two types of experimental environments were designed: normal scenarios and complex scenarios. Four mainstream grabbing methods were selected as comparison benchmarks, including the traditional model-based grabbing method (Method 1), the Half-Model-based method (Method 2), the robotic arm grabbing method based on point cloud segmentation (Method 3), and the robotic arm grabbing method based on deep reinforcement learning (Method 4). In normal scenarios, workpieces are arranged neatly and without obstructions, there are no unnecessary obstacles in the environment, and the workpiece types are single. In complex scenarios, workpieces

TABLE 2 Robot TCP calibration experiment.

Calibration point	Test ①x	Test ①y	Test ①z	Test ②x	Test ②y	Test ②z
1	434.85	−50.95	−266.10	437.10	−50.68	−264.65
2	436.75	−51.75	−264.40	436.20	−50.80	−264.35
3	436.55	−52.90	−266.45	436.65	−51.55	−264.70
4	436.30	−50.25	−265.70	437.15	−50.45	−265.10
TCP	290.50	−0.15	369.90	295.20	−0.90	371.00

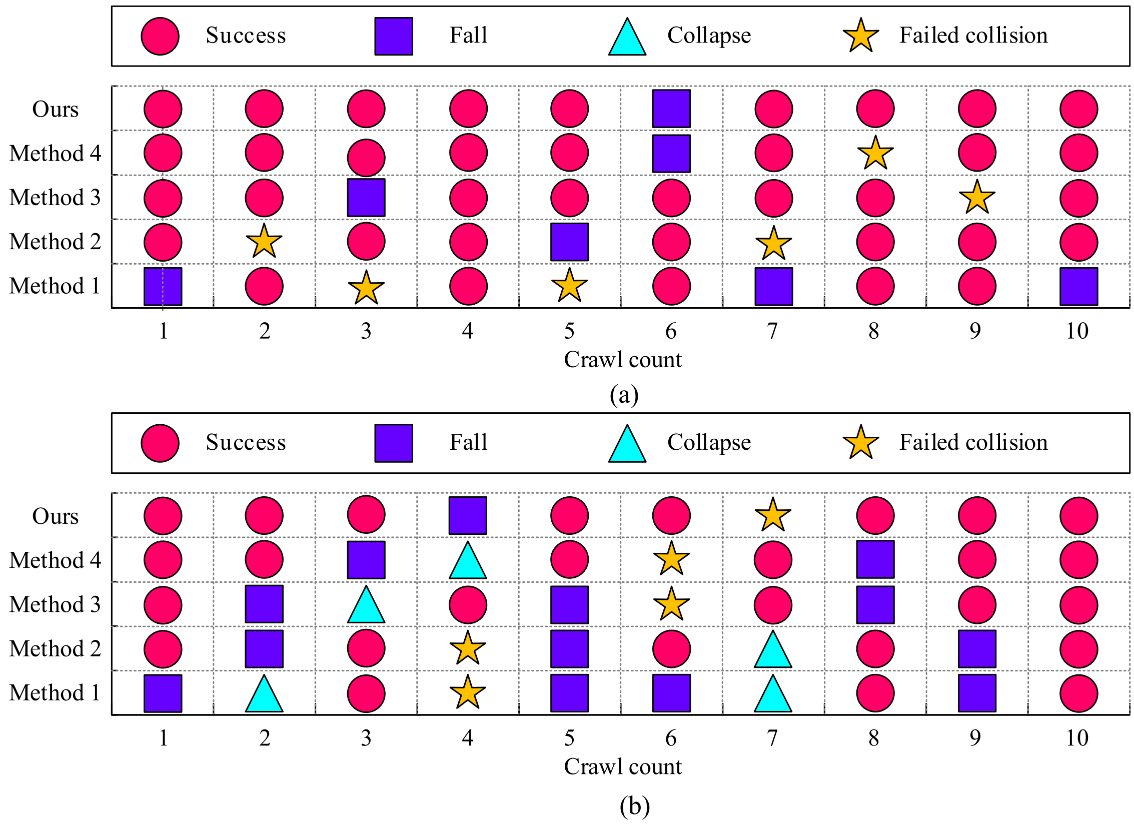

FIGURE 10
Capture results of five methods in normal scenarios/complex scenarios. **(a)** Five methods to capture results in normal scenarios. **(b)** Five methods to capture results in complex scenarios.

are randomly stacked and partially obscured, and there are interference objects such as tooling fixtures in the environment. Successful grabbing is defined as the robotic arm accurately gripping the workpiece and moving it to the designated position without the workpiece falling, collapsing, or colliding with the environment. Failure types include falling, collapsing, and collision. Dropping refers to the phenomenon where the workpiece is detached from the fixture due to insufficient clamping force or trajectory shaking after being held by the robotic arm. Collapse refers to the collapse of the stacked state of the workpiece due to the contact of the robotic arm, making it impossible to complete clamping. Collision failure refers to the rigid contact between the robotic arm and the workpiece, fixture, or environmental obstacle during its movement, resulting in the termination of the grasping task. To improve the reliability and statistical representativeness of the experimental results, a total of 100 grasping tests were conducted. Random sampling was used to select the 10th, 20th, 30th, 40th, 50th, 60th, 70th, 80th, 90th, and 100th test results for analysis. The 10 grasping results of the five methods under normal and complex scenarios are shown in Figure 10.

From Figure 10a, in the 10 sampling tests, only the 60th experiment showed the workpiece falling, and the remaining 9 times successfully completed the grasping task, demonstrating excellent grasping stability. From Figure 10b, in complex environments, the research method exhibited only a drop during the 40th grab operation and a collision during the 70th grab operation, without any collapse failures, demonstrating strong adaptability to workpiece stacking, occlusion, and interference

TABLE 3 Multi-dimensional performance evaluation results of five methods.

/	Grabbing efficiency (s/ times)	Anti-interference coefficient	Energy consumption cost (normalized)	Fixture wear rate (μm)
Traditional RRT	8.5	0.60	1.00	85.3
Half-model-based	7.2	0.77	0.92	72.6
RANSAC	6.8	0.79	0.88	68.9
DQN	9.3	0.75	1.15	92.1
Proposed model	5.5	0.89	0.75	45.2

conditions. To comprehensively evaluate the comprehensive performance of each method, the new grabbing efficiency (average time taken for a single grab), anti-interference coefficient (ratio of success rate between complex scenarios and normal scenarios), energy cost (average power consumption for a single grab), and fixture wear rate (deformation amount of the fixture after 100 consecutive grabs) are used to construct a multi-dimensional performance evaluation system. The anti-interference coefficient ≥0.8 is defined as strong anti-interference ability, 0.6–0.8 as medium anti-interference ability, and <0.6 as weak anti-interference ability. The division rules for anti-interference coefficients refer to the requirements for the adaptability of industrial robots to complex environments in GB/T 38326–2019 "Electromagnetic Compatibility Immunity Test for Industrial, Scientific and Medical Robots", combined with the quantitative criteria for environmental adaptability in IEEE related robot performance evaluation research. It is specifically designed for constructing factory robotic arm grasping scenarios, which not only conforms to industry standards but also adapts to the performance evaluation needs of normal and complex scenarios in experiments. The energy consumption cost is normalized using Method 1 as the benchmark value of 1.0. The experimental results are shown in Table 3.

From Table 3, the grabbing efficiency of the target product grabbing model based on digital twin technology was optimal, 19.1% higher than that of RANSAC. This is because the digital twin plans the optimal motion trajectory in advance and reduces the empty travel time of the robotic arm. The anti-interference coefficient reached 0.89, which belongs to the category of strong anti-interference ability. It was 18.7% higher than that of DQN, which reflected the adaptability of virtual and real synchronous perception to complex environments. The energy consumption cost was 25% lower than that of Traditional RRT, and the fixture wear rate was reduced by 47%.

4 Discussion and interpretation

Model performance test results showed that the joint motion stability data of the proposed model was significantly better than that of the traditional RRT algorithm. The angular velocity fluctuation amplitude narrowed from 0 to 60°/s to 0–15°/s, and the angular acceleration oscillation range converged from −500–500°/s^2 to −300–300°/s^2. The core reason lies in the offline pre-optimization capability of the digital twin. By completing trajectory iterative simulation in the virtual environment, motion singularities and velocity mutation points can be avoided in advance (Liu et al., 2023). The test results show that the angular velocity amplitude of the j4 and j5 joints is stable at 0–5°/s, without high-frequency jitter, the angular acceleration converges at −100–100°/s^2, there is no pulse oscillation, the rotation speed fluctuation range is controlled at −3~3°/s, and the entire process remains stable and synchronized. Industrial cameras and laser rangefinders jointly collect the three-dimensional coordinates of four calibration points. The over-determined equation system is constructed to solve the kinematic parameter errors, and the calibration deviation under different postures is simulated using digital twins to compensate for the errors caused by the joint clearance of the robotic arm and the deformation of the connecting rod in advance. The proposed model had a capture success rate of 90% in normal scenarios and 80% in complex scenarios, which were 10% and 20% higher than the optimal comparison method, respectively. The core function of collision detection is to avoid the collision risk between the robotic arm and the environment or workpiece in advance, and it does not directly achieve speed smoothness in essence. The speed smoothness of the proposed model mainly comes from the offline trajectory rehearsal of the digital twin, which can identify the speed mutation points in the path in advance, adjust the motion parameters to achieve speed gradient transition, and ultimately improve the smoothness of joint motion. In addition, the grabbing efficiency was 19.1% higher than that of the robotic arm grabbing method based on point cloud segmentation. This is because the digital twin plans the optimal motion trajectory in advance to reduce idle travel time. The energy consumption cost was reduced by 25% compared with the traditional method, and the fixture wear rate was reduced by 47%, which was a direct result of trajectory smoothness optimization. This optimization logic is highly consistent with the research paradigm of collaborative robot programming and control in the re-configurable production system proposed by Dimosthenopoulos et al. (2025). The RRT-Connect algorithm uses a bidirectional expansion strategy to construct a path tree. After the two path trees are connected, the path is optimized twice through the optimal parent node selection strategy. Taking the cumulative path cost from the starting point to the node as the objective function, the parent node that optimizes path smoothness is selected, effectively eliminating the inflection points and mutation segments that exist in traditional path planning, and forming a continuous and smooth joint motion curve.

As a random planner, RRT can efficiently search for paths in complex spaces, but it has inherent drawbacks such as high computational costs and the tendency to generate jagged paths, which are not conducive to improving industrial throughput. In addition, image data transmission and processing, and motion command parsing will generate millisecond delay, which may lead to trajectory execution deviation. Future research can optimize data processing flow through edge computing, shorten end-to-end delay, and improve real-time performance. Although the RRT-Connect algorithm adopts a bidirectional expansion strategy to improve path search efficiency for the common “narrow channel” working conditions in industrial scenarios, it is still prone to high randomness and uneven turning problems, which are also key issues that need to be addressed in industrial execution. Subsequent research can be conducted by pruning redundant inflection points and eliminating invalid path segments in the RRT-Connect path tree connection, combined with interpolation algorithms to smoothly transition path nodes, making joint motion curves continuous and differentiable, effectively solving the problem of uneven paths in narrow channels and adapting to industrial practical execution needs. The wear of industrial robots is a long-term fatigue indicator, and factory components typically perform thousands of cycles per day. Research measuring fixture deformation only after 100 cycles cannot fully reflect the wear pattern of fixtures throughout their entire lifecycle. Subsequently, by extending the testing cycle and combining fatigue wear theory, a fixture wear prediction model will be established to more accurately evaluate the long-term operational performance of fixtures, providing scientific basis for factory equipment maintenance and replacement.

The impact of the 4.88 mm TCP deviation on the precise positioning and grasping of the robotic arm is mainly reflected in two aspects. One is that for small precision target products, deviations may lead to grasping deviations, unstable clamping, and even damage to the product. The second is that under long-term operation, deviations will accumulate and transmit, reducing the consistency between the digital twin model and the actual robotic arm, and affecting grasping efficiency and stability. To control the TCP deviation within 3 mm, a physical calibration optimization scheme is adopted, which includes adjusting the geometric parameters of the robotic arm joints, re-optimizing the DH parameters based on high-precision calibration point data collected by the laser tracker, and correcting joint angle errors and link length errors. TCP is re-calibrated using a six point calibration method instead of a four point calibration method, increasing the number of collected calibration points and improving calibration accuracy. The data acquisition strategy of the laser tracker is optimized. The sampling frequency is increased to 1.5 kHz to reduce data acquisition lag, and the number of repetitions for each test group is increased from 2 to 5. The average TCP deviation is taken as the final result.

In response to the real-time safety hazards caused by the cumulative delay of 130 ms in the control circuit of the robotic arm, combined with its high motion speed of up to 600°/s, the reasonable design of the buffer zone is the key to avoiding collision risks and ensuring operational safety, especially in complex scenes with high obstacle density, which requires accurate calculation based on kinematic characteristics and scene constraints. The calculation logic for safe parking distance is based on the inertial motion distance of the robotic arm within a delay of 130 ms, combined with the joint motion characteristics, converting angular velocity into linear velocity, and calculating based on a uniform deceleration motion model. In complex scenarios, with high obstacle density and irregular distribution, buffer zone design needs to consider both parking distance and obstacle redundancy, adopting a layered buffering strategy. The inner layer is an emergency parking buffer zone, corresponding to the safe parking distance. The outer layer serves as a warning buffer zone, with an additional 0.3–0.5 m of redundancy reserved in combination with the density of obstacle distribution. Although this redundancy will occupy a small amount of work space, it can be dynamically adjusted through the digital twin virtual and real collaboration mechanism. The redundancy is reduced to 0.3 m in areas with sparse obstacles and maintained at 0.5 m in dense areas. This not only avoids the collision between multiple obstacles, but also minimizes the impact on the available work space in a tight factory environment, achieving a balance between safety and space utilization.

5 Conclusion

Aiming at the accuracy and efficiency bottlenecks of factory robotic arm target grabbing, a digital twin technology model including virtual and real communication, motion planning and grabbing execution was constructed, and the feasibility and superiority of the solution were verified through performance testing and scenario applications. The motion path performance test showed that the proposed model achieved significant optimization compared with the traditional RRT algorithm. The smoothness of the angular velocity curves of the j2 and j3 was greatly improved. The fluctuation amplitude narrowed from 0 to 60°/s in the traditional algorithm to 0–15°/s. The angular acceleration of the j1, j2, j3, and j6 was constrained to −300–300°/s^2, and the oscillation frequency and amplitude were significantly reduced. The rotation speed of the j1-j3 and j6 was stable at 6–7°/s, and stabilized in the later period. This indicates that the offline trajectory rehearsal of the digital twin and the path smoothing strategy of the RRT-Connect algorithm effectively suppress joint velocity mutations and impacts. The application effect test results showed that the average TCP coordinate deviation was 2.34 mm, which met the industrial ±3 mm accuracy requirement. The capture success rate in normal/complex scenarios reached 90% and 80%, respectively, which was significantly improved compared with mainstream methods. The capture efficiency was increased by 19.1%, and the energy consumption and fixture wear rate were reduced by 25% and 47%, respectively, achieving collaborative optimization of accuracy, efficiency and economy. Compared to methods 4 and 3 in the benchmark, the core advantages of the DT model are reflected in two points. One is the advantage of deterministic path planning and low-cost training. Although DRL methods are usually trained offline in simulated environments, their experimental phase relies on real-time trial and error and feedback iteration, which results in randomness and uncertainty. The DT model relies on the virtual real bidirectional synchronization mechanism to complete pre-planning and verification in the virtual space, output deterministic execution paths, and effectively avoid grasping conflicts. The second is the multi-dimensional collaborative optimization mechanism, which is superior to the point cloud segmentation method that only focuses on workpiece positioning, jointly optimizing trajectory planning, clamping control, and environmental adaptation, and improving the anti-interference ability of complex scenes. Although this research has achieved remarkable results, there are still limitations such as insufficient perception accuracy in complex environments and limited adaptability to heavy-load scenarios. In the future, the RRT algorithm can be improved through multi-sensor fusion and optimization of the perception module to improve path adaptability. A parametric modeling platform can be developed to shorten the adaptation cycle and provide support for the large-scale application of robotic arm grabbing technology in intelligent manufacturing scenarios.

Data availability statement

The original contributions presented in the study are included in the article/supplementary material, further inquiries can be directed to the corresponding author.

Author contributions

LC: Funding acquisition, Writing – original draft. XX: Conceptualization, Data curation, Writing – original draft. WM: Formal Analysis, Methodology, Writing – review and editing. PW: Formal Analysis, Software, Supervision, Writing – review and editing.

Funding

The author(s) declared that financial support was received for this work and/or its publication. The research is supported by Shanxi Provincial Basic Research Program (Free Exploration Category) 2023 Batch II Project: “Research on Casting-Rolling Forming and Interface Microstructure Evolution of Carbon Fiber-Reinforced Aluminum-Magnesium Matrix Composites (Grant No.: 202303021222290)”.

Conflict of interest

The author(s) declared that this work was conducted in the absence of any commercial or financial relationships that could be construed as a potential conflict of interest.

Generative AI statement

The author(s) declared that generative AI was not used in the creation of this manuscript.

Any alternative text (alt text) provided alongside figures in this article has been generated by Frontiers with the support of artificial intelligence and reasonable efforts have been made to ensure accuracy, including review by the authors wherever possible. If you identify any issues, please contact us.

Publisher’s note

References

Chen, S., Spyrakos-Papastavridis, E., Jin, Y., and Deng, Y. (2025). Goal-oriented semantic communication for robot arm reconstruction in digital twin: feature and temporal selections. *IEEE J. Sel. Areas Commun.* 43 (9), 3072–3087. doi:10.1109/JSAC.2025.3574592

Dawn, N., Ghosh, S., Saha, A., Chatterjee, S., Ghosh, T., Guha, S., et al. (2024). A review on digital twins technology: a new frontier in agriculture. *Artif. Intell. Appl.* 2 (4), 250–262. doi:10.47852/bonviewAIA3202919

Dimosthenopoulos, D., Basamakis, F. P., Glykos, C., Bavelos, A. C., Mountzouridis, G., and Makris, S. (2025). A Digital Twin-based paradigm for programming and control of cooperating robots in reconfigurable production systems. *Int. J. Comput. Integr. Manuf.* 38 (10), 1443–1463. doi:10.1080/0951192X.2024.2428683

Duan, J., Gong, X., Zhang, Q., and Qin, J. (2023). A digital twin–driven monitoring framework for dual-robot collaborative manipulation. *Int. J. Adv. Manuf. Technol.* 125 (9), 4579–4599. doi:10.1007/s00170-023-11064-2

Gao, N., and Lu, Q. (2024). Big data analysis and deep learning optimization in artificial intelligence production of information enterprises. *Scalable Comput. Pract. Exp.* 25 (3), 1533–1540. doi:10.12694/scpe.v25i3.2703

Inamura, T. (2023). Digital twin of experience for human–robot collaboration through virtual reality. *Int. J. Automation Technol.* 17 (3), 284–291. doi:10.20965/ijat.2023.p0284

Jiao, Q., Hu, W., Hao, G., Cheng, J., Peng, X., Liu, Z., et al. (2025). A digital twin of intelligent robotic grasping based on single-loop-optimized differentiable architecture search and sim-real collaborative learning. *J. Intelligent Manuf.* 36 (8), 5903–5922. doi:10.1007/s10845-024-02498-w

Liao, Z., and Cai, Y. (2024). AR-enhanced digital twin for human–robot interaction in manufacturing systems. *Energy, Ecol. Environ.* 9 (5), 530–548. doi:10.1007/s40974-024-00327-7

Liu, D., Chen, Y., and Wu, Z. (2023). Digital twin (Dt)-cyclegan: enabling zero-shot sim-to-real transfer of visual grasping models. *IEEE Robotics Automation Lett.* 8 (5), 2421–2428. doi:10.1109/LRA.2023.3254460

Peng, W., Wang, W., Wang, Y., Zhang, H., Mao, J., Liu, M., et al. (2024). Key technologies and trends of active robotic 3-D measurement in intelligent manufacturing. *IEEE/ASME Trans. Mechatronics* 29 (6), 4778–4799. doi:10.1109/TMECH.2024.3396222

Ren, L., Dong, J., Huang, D., and Lü, J. (2023). Digital twin robotic system with continuous learning for grasp detection in variable scenes. *IEEE Trans. Industrial Electron.* 71 (7), 7653–7663. doi:10.1109/TIE.2023.3299049

Rivera-Pinto, A., Kildal, J., and Lazkano, E. (2024). Toward programming a collaborative robot by interacting with its digital twin in a mixed reality environment. *Int. J. Human–Computer Interact.* 40 (17), 4745–4757. doi:10.1080/10447318.2023.2221599

Singh, O., and Ray, A. K. (2024). A physical-virtual based digital twin robotic hand. *Int. J. Interact. Des. Manuf.* 18 (7), 4829–4839. doi:10.1007/s12008-024-01773-7

Stan, L., Nicolescu, A. F., Pupăză, C., and Jiga, G. (2023). Digital Twin and web services for robotic deburring in intelligent manufacturing. *J. Intelligent Manuf.* 34 (6), 2765–2781. doi:10.1007/s10845-022-01928-x

Touhid, M. T. B., Marne, M., Oskroba, T., Mirahmadi, S. A., Zhu, E., Mehrabian, A., et al. (2023). Building a cloud-based digital twin for remote monitoring and control of a robotic assembly system. *Int. J. Adv. Manuf. Technol.* 129 (9), 4045–4057. doi:10.1007/s00170-023-12611-7

Tsakoumis, D., Koronakos, G., Plitsos, S., Feik, J., and Eirinakis, P. (2025). Optimizing energy consumption of robotic arm movements based on digital twins. *IFAC-PapersOnLine* 59 (10), 1396–1401. doi:10.1016/j.ifacol.2025.09.235

Wang, X., Hua, Y., Gao, J., Lin, Z., and Yu, R. (2023). Digital twin implementation of autonomous planning arc welding robot system. *Complex Syst. Model. Simul.* 3 (3), 236–251. doi:10.23919/CSMS.2023.0013

Wang, K., Wang, X., Tan, C., Dong, S., Zhao, F., and Lian, S. (2025). Digital twin-enhanced robotic system for remote diesel engine assembly defect inspection. *Industrial Robot* 52 (2), 266–276. doi:10.1108/IR-05-2024-0215

Wu, Z., Yao, Y., Liang, J., Jiang, F., Chen, S., Zhang, S., et al. (2023). Digital twin-driven 3-D position information mutuality and positioning error compensation for robotic arm. *IEEE Sensors J.* 23 (22), 27508–27516. doi:10.1109/JSEN.2023.3315302

Yang, G., Ye, Z., Wu, H., Li, C., Wang, R., Kong, D., et al. (2024). A digital twin-based large-area robot skin system for safer human-centered healthcare robots toward healthcare 4.0. *IEEE Trans. Med. Robotics Bionics* 6 (3), 1104–1115. doi:10.1109/TMRB.2024.3421635